

# Quantum Zeno effect and quantum nondemolition spin measurement in a quantum dot–micropillar cavity in the strong coupling regime

N. V. Leppenen <sup>1</sup>, L. Lanco,<sup>2,3</sup> and D. S. Smirnov <sup>1,\*</sup>

<sup>1</sup>*Ioffe Institute, 194021 St. Petersburg, Russia*

<sup>2</sup>*Centre for Nanosciences and Nanotechnology, CNRS, Universite Paris-Saclay, UMR 9001, 10 Boulevard Thomas Gobert, 91120 Palaiseau, France*

<sup>3</sup>*Universite Paris Diderot - Paris 7, 75205 Paris Cedex 13, France*



(Received 18 August 2020; revised 27 November 2020; accepted 23 December 2020; published 14 January 2021)

We theoretically describe the quantum Zeno effect in a spin-photon interface represented by a charged quantum dot in a micropillar cavity in the strong coupling regime. This simplest model allows for various generalizations for the different systems. We derive a simple expression for the spin measurement rate, which allows one to tune the electron spin precession frequency in an external magnetic field and spin relaxation time. We calculate the spin noise bispectrum, which reveals the qualitative change of the spin dynamics with an increase of the measurement strength and proves the quantum nature of the spin noise. We also calculate the quantum information gain rate and find the conditions when it equals the spin dephasing rate, i.e., reaches the quantum limit.

DOI: [10.1103/PhysRevB.103.045413](https://doi.org/10.1103/PhysRevB.103.045413)

## I. INTRODUCTION

The quantum Zeno effect in the most spectacular way shows the fundamental difference between the quantum microscopic world and the classical everyday life. Explicitly, it states that a continuously observed quantum object cannot move [1,2]. After being formulated as a paradox for classical objects by Zeno of Elea in the 5th century BC [3], it was later described as a physical effect for the quantum objects in the most popular way in 1977 [4].

Nowadays many aspects of the quantum Zeno effect are under active investigation [5,6]. These include, for example, deceleration of the quantum dynamics under continuous weak measurement [7], quantum anti-Zeno effect [8,9], dynamics in the quantum Zeno subspaces [10], and observation of the quantum Zeno effect in various systems from free atoms to semiconductors [11–18]. The general interest is additionally boosted by the importance of this effect for quantum computation [19–23]. The quantum Zeno effect on one hand can help to increase the storage time of quantum information [24], but on the other hand it can slow down or even damage the computations [25,26].

In parallel to the mainly theoretical investigations of the quantum Zeno effect, there is a growing interest in the realization of a spin-photon interface. It has a large number of applications including spin-photon gates, spin-mediated photon-photon gates, and emission of a photonic cluster state with a wide range of applications for quantum information processing [27–31]. These applications are based on the entanglement between photon and electron spins during the interaction, which can be strongly enhanced by optical

microcavities. Recently, we demonstrated that even single photon detection can lead to significant backaction on the electron spin [32].

When the electron spin is subject to a continuous interaction with light, many photons get entangled with a single electron spin, so it is natural to expect the quantum Zeno effect. Its theoretical description is an important step towards the realization of quantum information processing. In this paper we consider the simplest, almost textbook realization of the spin-photon interface, which is represented by a quantum dot (QD)–micropillar cavity with a resident electron in the QD. The fastest spin manipulation and electron photon entanglement are reached in the strong coupling regime, when hybrid polariton modes are formed in the micropillar [33]. The fabrication of such devices remained elusive until recently [34]. Despite a few theoretical proposals for the efficient spin control and nearly nonperturbing spin measurement in the QD micropillar cavity in the strong coupling regime [32,35], the theory of electron spin dynamics under the conditions of the quantum Zeno effect in this structure is still missing.

Our paper is organized as follows. In the next section we formulate the model of the device under study. Then in Sec. III we describe the quantum Zeno effect using three independent approaches—phenomenological, numerical, and analytical—and establish the relation between them. In Sec. IV we calculate the quantum nondemolition spin measurement rate, relate it with the entanglement between electron and photon spins, and compare it with the spin dephasing rate. We also find the conditions when the quantum limit for the spin measurement is reached. Finally, in Sec. V we study the statistics of the spin noise and calculate the noise bispectrum. The applicability of our findings to realistic devices and possible extensions of our simplest model, as well as a brief summary, are presented in Sec. VI.

\*smirnov@mail.ioffe.ru

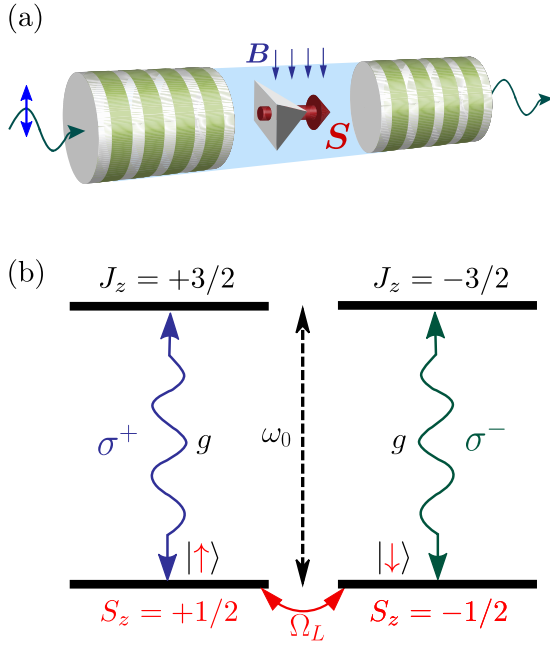


FIG. 1. (a) Sketch of a QD micropillar cavity with a single electron with the spin  $S$  in an external magnetic field  $B$  with the incident linearly polarized probe light. (b) Energy levels of the QD: two ground electron spin states with  $S_z = \pm 1/2$  and two singlet trion states with heavy hole spin  $J_z = \pm 3/2$  as well as the allowed optical transitions between them.

## II. MODEL

We consider a micropillar cavity with a QD inside it [Fig. 1(a)]. We assume that the QD is charged with a single electron. The device is placed in an external transverse magnetic field (perpendicular to the structure growth axis  $z$ ) and coherently excited by a continuous linearly polarized light.

The Hamiltonian of the system has the form [32,35]

$$\mathcal{H} = \mathcal{H}_+ + \mathcal{H}_- + \mathcal{H}_B. \quad (1)$$

The first two terms describe the contributions with right-handed and left-handed helicities (signs of the angular momentum projections on the  $z$  axis):

$$\begin{aligned} \mathcal{H}_{\pm} = & \hbar\omega_c c_{\pm}^{\dagger} c_{\pm} + \hbar\omega_0 a_{\pm 3/2}^{\dagger} a_{\pm 3/2} \\ & + \hbar(gc_{\pm} a_{\pm 3/2}^{\dagger} a_{\pm 1/2} + \mathcal{E}_{\pm} e^{-i\omega t} c_{\pm}^{\dagger} + \text{H.c.}). \end{aligned} \quad (2)$$

Here,  $c_{\pm}$  ( $c_{\pm}^{\dagger}$ ) are the annihilation (creation) operators of the  $\sigma^{\pm}$  photons in the cavity. The two orthogonally polarized cavity modes have an eigenfrequency  $\omega_c$ , and they are assumed to be degenerate. In the devices available to date there is a large splitting between the two linearly polarized cavity modes [34,36]. In order to optically control the electron spin and directly apply the theory presented below, this splitting should be reduced to a value below the cavity mode decay rate. The QD is described by four states with the corresponding annihilation operators  $a_{\pm 1/2}$  and  $a_{\pm 3/2}$ . The former two correspond to the two ground electron states with a spin projection  $S_z = \pm 1/2$ . The latter two correspond to the excited singlet trion states with an energy  $\hbar\omega_0$  [see Fig. 1(b)]. The trion consists of two electrons with opposite spins and a heavy hole

with a spin  $J_z = \pm 3/2$ . Further,  $g$  is the light-matter coupling strength. It describes the photon absorption from the cavity mode and the creation of a trion from a single electron, as well as the reverse process. According to the optical selection rules, the total angular momentum component along the  $z$  axis is conserved, so the absorption of the  $\sigma^{\pm}$  photon is accompanied by the creation of a hole with  $J_z = \pm 3/2$  and an electron with  $S_z = \mp 1/2$ , respectively [37] [see Fig. 1(b)]. Due to the Pauli exclusion principle this is possible only when the resident electron in the QD has  $S_z = \pm 1/2$ , as described by Eq. (2). Finally, the parameters  $\mathcal{E}_{\pm}$  are proportional to the amplitudes of the  $\sigma^{\pm}$  polarized components of the coherent incident light with frequency  $\omega$  [38]. We consider the system excitation by linearly polarized light, which corresponds to  $\mathcal{E}_+ = \mathcal{E}_- = \mathcal{E}$ .

The effect of the external magnetic field is described by

$$\mathcal{H}_B = \frac{\hbar\Omega_L}{2} \sum_{\pm} a_{\pm 1/2}^{\dagger} a_{\mp 1/2}, \quad (3)$$

where  $\Omega_L$  is the Larmor frequency of the electron. The transverse Landé factor of the heavy hole is very small [39], so we neglect it.

The system under study is open, and it should be described using the density matrix formalism. The density matrix  $\rho(t)$  satisfies the master equation

$$\dot{\rho}(t) = \frac{i}{\hbar} [\rho(t), \mathcal{H}] - \mathcal{L}\{\rho(t)\}, \quad (4)$$

where the dot denotes the time derivative and the Lindblad superoperator  $\mathcal{L}\{\rho(t)\}$  describes the incoherent processes [38]. We take into account only two of them: nonradiative trion decay with the rate  $2\gamma$  and the photon escape from the cavity with the rate  $2\kappa$ . They are described by

$$\begin{aligned} \mathcal{L}\{\rho\} = & \sum_{\pm} [\kappa(c_{\pm}^{\dagger} c_{\pm} \rho + \rho c_{\pm}^{\dagger} c_{\pm} - 2c_{\pm} \rho c_{\pm}^{\dagger}) \\ & + \gamma(a_{\pm 3/2}^{\dagger} a_{\pm 3/2} \rho + \rho a_{\pm 3/2}^{\dagger} a_{\pm 3/2} \\ & - 2a_{\pm 1/2}^{\dagger} a_{\pm 3/2} \rho a_{\pm 3/2}^{\dagger} a_{\pm 1/2})]. \end{aligned} \quad (5)$$

Note that  $\gamma$  can also account for the radiative trion recombination, if the photon is not emitted into the cavity mode. We assume that the trion recombination conserves the helicity, so after the recombination of a trion with  $J_z = \pm 3/2$ , a  $\sigma^{\pm}$  polarized photon is emitted and an electron with  $S_z = \pm 1/2$  is left in the QD [see Fig. 1(b)]. The cavity mode decay rate is contributed by the photon escape through the left and right mirrors and through the side walls:  $\kappa = \kappa_1 + \kappa_2 + \kappa_0$ , respectively. We assume that the light is incident at the cavity from the left. The amplitude transmission coefficient through the left (right) mirror is proportional to the square root of  $\kappa_1$  ( $\kappa_2$ ) [40].

For the rest of the paper we assume perfect tuning between the trion resonance frequency and the cavity mode,  $\omega_c = \omega_0$ , and stick to the notation  $\omega_0$ . Moreover, we limit ourselves to the weak magnetic and driving fields:

$$\Omega_L, \mathcal{E} \ll \kappa. \quad (6)$$

The lowest eigenstates of the system and transitions between them, taking into account the interaction with the cavity in the strong coupling regime, are shown in Fig. 2. The two ground

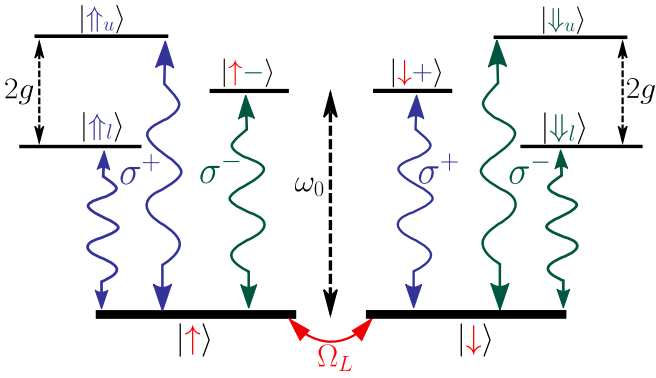


FIG. 2. The lowest energy levels of the system and optical transitions between them. The electron spin states are denoted by the red vertical arrows, the  $\pm$  sign refers to the  $\sigma^\pm$  polarization of a single photon, and the polariton states are defined in Eqs. (7).

spin states, which are mixed by the magnetic field, are mostly populated.

The lowest excited states are the single photon states and the polariton states [33]. If a single  $\sigma^\pm$  photon is present in the cavity and the electron is in the spin-down/up state, respectively, then the photon cannot be absorbed, as described above and shown in Fig. 1(b), and this is an eigenstate. These states are shown in the middle of Fig. 2. In the opposite case, when the electron and photon have the same helicities, multiple photon absorption and reemission by the QD leads to the formation of polariton states. In the case under study ( $\omega_c = \omega_0$ ) they have the form

$$|\uparrow_\gamma\rangle = \frac{a_{+3/2}^\dagger \pm c_+^\dagger}{\sqrt{2}}|0\rangle, \quad |\downarrow_\gamma\rangle = \frac{a_{-3/2}^\dagger \pm c_-^\dagger}{\sqrt{2}}|0\rangle, \quad (7)$$

where  $|0\rangle$  denotes the vacuum state, and the subscripts  $u, l$  refer to the upper and lower polariton states, respectively. These states have the energies

$$E_{u,l} = \hbar(\omega_0 \pm g), \quad (8)$$

as shown in Fig. 2. The polariton states (7) are well defined states in the strong coupling regime only, when the damping is smaller than the splitting:  $\gamma, \varkappa \ll g$ . In this paper we mainly focus on this regime, but the formalism developed below is valid for the weak coupling regime as well. However, the quantum Zeno effect in the weak coupling regime can be described without taking into account the quantization of the electromagnetic field [41,44].

For weak incident light [Eq. (6)] the system is mainly in the Hilbert space of the two electron spin states and vacuum photon state. In this case, the amplitude transmission coefficient of circularly polarized light is equal to

$$t_0 = \frac{i\varkappa}{\omega - \omega_0 + i\varkappa} \quad (9a)$$

for  $\sigma^\pm$  polarized light and a spin-down/up electron, respectively. The intensity transmission coefficient  $T_0 = |t_0|^2$  is shown in Fig. 3 as a function of the detuning  $\omega - \omega_0$ . It has a Lorentzian shape with the maximum at a bare cavity frequency  $\omega_0$ . It describes the resonant transmission of the circularly polarized light for the case when its interaction

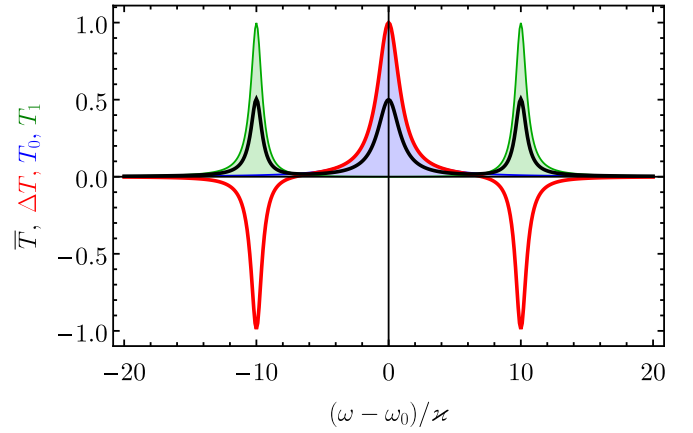


FIG. 3. Contributions to the total intensity transmission coefficient  $\bar{T}$  and  $\Delta T$  [see Eq. (10)] (black and red curves, respectively) and the transmission coefficients  $T_{0,1}$  (blue and green areas, respectively) calculated after Eqs. (9) with the parameters  $\gamma = 0$  and  $g/\varkappa = 10$ .

with the QD is forbidden by the optical selection rules. In the opposite case of  $\sigma^\mp$  polarized light and a spin-down/up electron, respectively, the amplitude transmission coefficient is [38,42]

$$t_1 = \frac{i\varkappa}{\omega - \omega_0 + i\varkappa - \frac{g^2}{\omega - \omega_0 + i\gamma}}. \quad (9b)$$

In this case, the intensity transmission coefficient  $T_1 = |t_1|^2$  describes the resonant light transmission at the polariton energies [Eq. (8)] for the case when the circularly polarized photons can be absorbed by the QD. Typically, the trion decay rate is much smaller than the photon escape rate [36], so in Fig. 3 we consider the limit  $\gamma = 0$ . In this limit, the widths of the peaks in  $T_1$  are two times smaller than that in  $T_0$ , because the polariton consists of the photon only by one half, so its amplitude decay rate is two times smaller than  $\varkappa$ .

Generally, the intensity transmission coefficients of the  $\sigma^\pm$  polarized light depend on the electron spin as [35]

$$T_\pm = \bar{T} \pm \Delta T S_z, \quad (10)$$

where  $\bar{T} = (T_0 + T_1)/2$  and  $\Delta T = T_1 - T_0$ . These transmission coefficients are also shown in Fig. 3.

Equation (10) shows that the transmission coefficient of circularly polarized light depends on the electron spin orientation. The circular polarization degree of the transmitted light for the linearly polarized incident light is proportional to the electron spin polarization:

$$S_z(t) \propto I_+(t) - I_-(t) \equiv \Delta I(t). \quad (11)$$

Here,  $I_\pm(t)$  are the intensities of the transmitted  $\sigma^\pm$  polarized light, and we introduced  $\Delta I(t)$ . This is also called the spin induced ellipticity of the transmitted light [43].

In the steady state, the average spin polarization is absent:  $\langle S_z(t) \rangle = 0$ . Hereafter the angular brackets denote the quantum statistical average. In this case, the spin dynamics is characterized by the spin correlation function  $\langle S_z(t) S_z(t + \tau) \rangle$  [44]. In the steady state it does not depend on  $t$ , so in the following we write it as  $\langle S_z(0) S_z(\tau) \rangle$ . From Eq. (11) one can

see that it is given by the correlation function of the circular polarization:

$$\langle S_z(0)S_z(\tau) \rangle \propto \langle \Delta I(0)\Delta I(\tau) \rangle. \quad (12)$$

Detection of the correlation functions is known as the spin noise spectroscopy [44], and this is a particular case of the ellipticity measurement of the transmitted light.

The same time spin correlation functions for a single electron simply read [44]

$$\langle S_\alpha(0)S_\beta(0) \rangle = \frac{\delta_{\alpha,\beta}}{4}, \quad (13)$$

where  $\alpha, \beta = x, y, z$  and  $\delta_{\alpha,\beta}$  is the Kronecker symbol. The correlation function  $\langle S_z(0)S_z(\tau) \rangle$  is an even function of  $\tau$  and for  $\tau > 0$  it satisfies the same equation of motion as  $S_z(\tau)$  [45]. For this reason the spin correlation function gives direct access to the spin dynamics and reveals the quantum Zeno effect even in the case when the average spin polarization is absent.

### III. QUANTUM ZENO EFFECT

The quantum Zeno effect is natural to expect under a continuous electron spin measurement. However, the microscopic description of this effect is absent for the system under study. Here, we use the phenomenological, numeric, and analytical approaches to describe this effect. As a result, we obtain a simple expression which allows one to tune the strength of the backaction by changing the intensity and frequency of the probe light.

#### A. Phenomenological approach

Here, we present a simple phenomenological approach to the quantum Zeno effect. Its validity for the system under study will be rigorously proven using the numerical and analytical approaches in the following sections.

A single electron spin precession in the external magnetic field applied along the  $x$  axis is generally described by the Hamiltonian

$$\mathcal{H}_0 = \hbar\Omega_L\sigma_x/2, \quad (14)$$

where we use a vector composed of the spin Pauli matrices  $\sigma = (\sigma_x, \sigma_y, \sigma_z)$ . Phenomenologically, the continuous weak measurement of the spin component  $S_z$  is described by the following equation for the  $2 \times 2$  spin density matrix  $\rho(t)$  [46,47],

$$\dot{\rho}(t) = -\frac{i}{\hbar}[\mathcal{H}_0, \rho(t)] - \frac{\lambda}{2}[\sigma_z, [\sigma_z, \rho(t)]], \quad (15)$$

where the second term describes the measurement of the spin  $z$  component with the phenomenological ‘‘measurement strength’’  $\lambda$ . It leads to the continuous decay of the spin components  $S_x$  and  $S_y$  which do not commute with the observable  $S_z$  due to the measurement backaction. The measurement can be associated with the quickly fluctuating magnetic field along the  $z$  axis, which is provided by the randomly incoming and outgoing photons due to the dynamic Zeeman effect [48,49]. This is a quite general situation, so one can expect that this model correctly describes different ways of the spin measurement. Note that here we use the Markovian approximation, so

the quantum anti-Zeno effect does not take place in this model [50,51].

The electron spin is given by  $S(t) = \text{Tr}[\rho(t)\sigma/2]$ , and from Eq. (15) we obtain the kinetic equations

$$\dot{S}_x = -2\lambda S_x, \quad \dot{S}_y = -\Omega_L S_z - 2\lambda S_y, \quad \dot{S}_z = \Omega_L S_y. \quad (16)$$

These equations describe the electron spin precession around the magnetic field and relaxation of the spin components  $S_x$  and  $S_y$ , which do not commute with the observable  $S_z$  due to the measurement backaction [52,53].

From the two latter equations we obtain the two complex eigenfrequencies of the spin dynamics

$$\Omega_{\pm}^* = \pm\sqrt{\Omega_L^2 - \lambda^2} - i\lambda. \quad (17)$$

For the weak measurement strength  $\lambda < \Omega_L$  the frequencies have opposite real parts and the same imaginary part  $\lambda$ . This describes the damped spin oscillations. With an increase of the measurement strength, the absolute values of the real parts of the eigenfrequencies decrease and eventually become zero. For the strong measurement there are no spin oscillations and the spin decays as an overdamped oscillator.

From the solution of Eqs. (16) we obtain

$$S_z(t) = S_z(0) \left[ \cos(\Omega t) + \frac{\lambda}{\Omega} \sin(\Omega t) \right] e^{-\lambda t} + S_y(0) \frac{\Omega_L}{\Omega} \sin(\Omega t) e^{-\lambda t}, \quad (18)$$

where  $\Omega = \sqrt{\Omega_L^2 - \lambda^2}$  is the reduced spin precession frequency. This expression shows that the quantum Zeno effect leads to the decrease of the spin precession frequency  $\Omega$  and induces the spin relaxation. Qualitatively, this effect was observed for an ensemble of electrons in the planar microcavity [41]. Note that it can also be called a watchdog effect [54].

The spin correlation functions can be calculated using a number of methods [44]. For the following it is useful to apply the formalism of the Kraus operators of the form

$$K(s) = \left( \frac{2\eta}{\pi} \right)^{1/4} e^{-\eta(s-S_z)^2}, \quad (19)$$

where  $s$  is a continuous real parameter and  $\eta$  tends to zero for a weak continuous spin measurement [55]. To calculate the correlator  $\langle S_z(0)S_z(\tau) \rangle$  for  $\tau > 0$  we solve the master equation (15) with the initial condition

$$\rho(0) = K(s_1)\rho_0K(s_1), \quad (20)$$

which represents the steady state density matrix weakly modified by the action of the measurement at  $t = 0$  with  $\rho_0$  being proportional to the identity matrix. The measurement at  $t = \tau$  similarly weakly changes the density matrix to

$$\rho_2 = K(s_2)\rho(\tau)K(s_2). \quad (21)$$

Then the spin correlation function is given by

$$\langle S_z(0)S_z(\tau) \rangle = \iint s_1 s_2 \text{Tr}[\rho_2] ds_1 ds_2, \quad (22)$$

where the limit  $\eta \rightarrow 0$  should be taken. The calculation yields [55,56]

$$\langle S_z(0)S_z(t) \rangle = \frac{1}{4} \left[ \cos(\Omega t) + \frac{\lambda}{\Omega} \sin(\Omega|t|) \right] e^{-\lambda|t|}. \quad (23)$$

This correlation function can be directly measured experimentally, as described in the previous section.

Interestingly, it was suggested that with an increase of the spin measurement strength, the spin dynamics undergo a quantum dynamical phase transition due to the quantum Zeno effect [57]. The transition can be evidenced in the modification of the counting statistics, which is described by the generating functions [58]. They satisfy the Schrödinger-like equation with the non-Hermitian Hamiltonian. The eigenspectrum of this Hamiltonian can be described by a certain braid group [59]. At the measurement strength  $\lambda = \Omega_L$  the braid group of the eigenspectrum changes, so the spin dynamics arguably undergoes the topological phase transition. Moreover, one can show that the braid group changes also at  $\lambda/\Omega_L \approx 0.65$  and  $0.18$ . This may correspond to the two additional phase transitions, which, however, were predicted to take place at  $\lambda/\Omega_L = 0.58$  and  $0.5$  [60]. In this paper we will not study this contradiction.

The description of the quantum Zeno effect presented in this section is phenomenological. In the next sections we prove that it can correctly describe the spin dynamics in the QD micropillar cavity and derive the microscopic expression for the phenomenological measurement strength  $\lambda$ .

## B. Numerical approach

Here, we present the numerical results obtained in the density matrix formalism based on the solution of the master equation (4) and compare them with the phenomenological theory described above.

The electron spin cannot be measured directly, but only using the photons as described in Sec. II. For this reason we study in this section the polarization of the transmitted light. The intensity of the transmitted  $\sigma^\pm$  polarized light is proportional to the number of corresponding photons in the cavity,  $I_\pm(t) \propto c_\pm^\dagger(t)c_\pm(t)$ , so  $\Delta I(t) \propto \Delta n(t)$ , where

$$\Delta n(t) = c_+^\dagger(t)c_+(t) - c_-^\dagger(t)c_-(t). \quad (24)$$

Thus the correlator  $\langle S_z(0)S_z(t) \rangle$  in Eq. (12) is proportional to the correlator of  $\Delta n(t)$  given by

$$\langle \Delta n(0)\Delta n(t) \rangle = 2(\langle c_+^\dagger(0)c_+^\dagger(t)c_+(t)c_+(0) \rangle - \langle c_+^\dagger(0)c_-^\dagger(t)c_-(t)c_+(0) \rangle), \quad (25)$$

where we used the fact that  $\Delta n(t)$  is zero on average and took into account the normal and time ordering of the operators [40].

In Eq. (25) the creation and annihilation operators in the Heisenberg representation are used. However, in the numerical calculations it is more convenient to switch to the Schrödinger representation and to solve Eq. (4) for the time dependent density matrix.

The numerical calculation of Eq. (25) consists of three steps:

- (i) We find the density matrix  $\rho_0$  for the steady state.

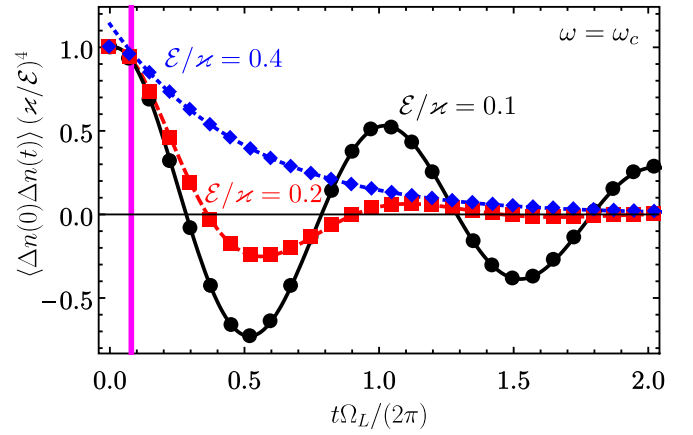


FIG. 4. Dimensionless correlation function of the circular polarization degree of the transmitted light calculated numerically with the parameters  $\omega = \omega_0$  and  $\gamma = 0$  in the limit  $g \gg \varkappa$  for different amplitudes of the incident light given in the labels with the corresponding color. The curves show the fits after Eq. (30). The vertical magenta line shows the time  $t = 5/\varkappa$ .

- (ii) Following the quantum regression theorem [40], we calculate the density matrix of the system after a single  $\sigma^+$  photon detection

$$\rho(0) = c_+\rho_0c_+^\dagger. \quad (26)$$

It represents the action of the two outer operators in Eq. (25).

- (iii) We find the solution  $\rho(t)$  of the master equation (4) with the initial condition (26). Then the correlators in Eq. (25) are given by

$$\langle c_+^\dagger(0)c_\pm^\dagger(t)c_\pm(t)c_+(0) \rangle = \text{Tr}[c_+\rho(t)c_+^\dagger]. \quad (27)$$

As a result, the correlator of the photon numbers reads

$$\langle \Delta n(0)\Delta n(t) \rangle = 2\{\text{Tr}[c_+^\dagger c_+\rho(t)] - \text{Tr}[c_-^\dagger c_-\rho(t)]\}. \quad (28)$$

This approach is exact and valid for the arbitrary relation between the parameters of the system. To speed up the numerical calculations, we consider the strong coupling regime and coherent excitation in the vicinity of the bare cavity resonance frequency:

$$|\omega - \omega_0|, \varkappa, \gamma \ll g. \quad (29)$$

In this limit we can neglect the polariton states and consider only the states that are the product of the QD ground state and photon Fock states. In the numerical calculation we consider the states with up to six photons and we checked that for 12 photons the results are the same. This allows us to perform the exact calculations beyond the limit (6).

In Fig. 4 we show with the dots the correlator  $\langle \Delta n(0)\Delta n(t) \rangle$  as a function of  $t$  for the different amplitudes of the incident light  $\mathcal{E}$ . It indeed resembles the spin correlation function, Eq. (23): It shows the damped oscillations. For this reason we fit  $\langle \Delta n(0)\Delta n(t) \rangle$  with an expression

$$\text{Re}(Ae^{-i\Omega^*t}), \quad (30)$$

where  $A$  and  $\Omega^*$  are the complex fit parameters. The fits are shown in Fig. 4 by the curves of the corresponding color. One can see that the fits nicely describe the numerical results for

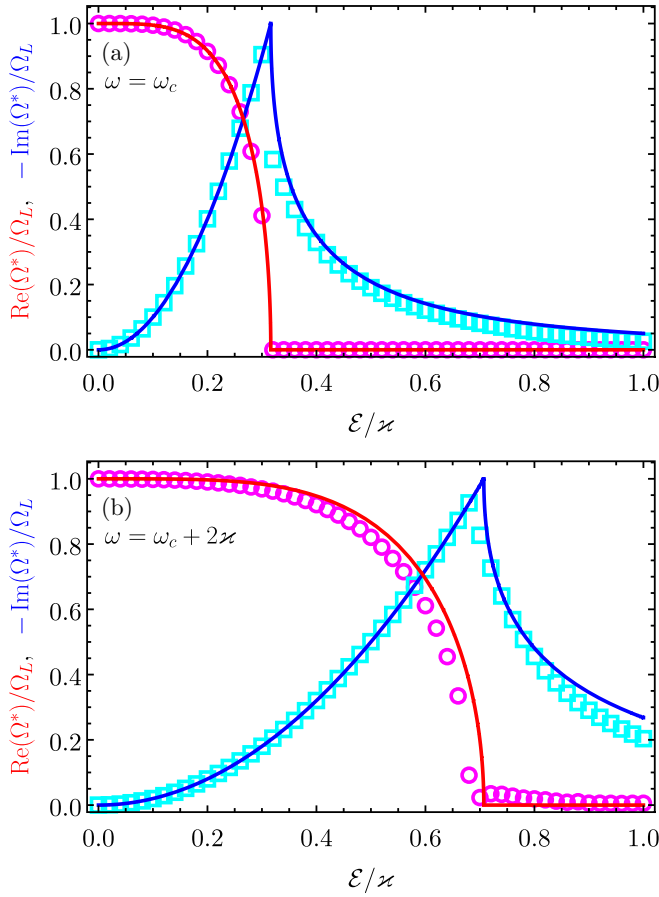


FIG. 5. The spin precession frequency (red circles) and spin relaxation rate (blue squares) as functions of the amplitude of the incident light. The parameters of the calculation in (a) are the same as in Fig. 4 and in (b) they are the same except for  $\omega = \omega_c + 2\kappa$ . The curves are calculated after Eqs. (17) and (42) with the same parameters.

the time  $t > 5/\kappa$ . At shorter timescales the photon-photon interaction modifies the photon correlation functions [32].

We show the fit parameters  $\text{Re}(\Omega^*)$  and  $-\text{Im}(\Omega^*)$  in Fig. 5 by circles and squares, respectively, as functions of the amplitude of the incident light. One can see that they show similar behavior for the different frequencies of the light [Figs. 5(a) and 5(b)]: The precession frequency  $\text{Re}(\Omega^*)$  monotonously decreases with an increase of  $\mathcal{E}$  and becomes zero after a certain threshold. The spin relaxation rate  $-\text{Im}(\Omega^*)$  first increases with an increase of the intensity of the light, and then decreases after the threshold. In the limit of large power of the probe light,  $\mathcal{E} \rightarrow \infty$ , we obtain  $\Omega^* = 0$ , which evidences the spin “freezing” due to the quantum Zeno effect under a strong continuous spin measurement.

We have checked that the presented dependencies are qualitatively the same for any choice of the system parameters. We have also checked that the relation  $|\Omega^*| = \Omega_L$  is satisfied below the threshold in agreement with Eq. (17). This shows that the phenomenological model of the quantum Zeno effect described in the previous section is valid for the system under study and that this effect can be observed in the intensity correlation functions of the transmitted light. In the next section

we derive an analytical expression for the spin measurement strength  $\lambda$ .

### C. Analytical approach

For the weak incident light and small magnetic field [Eq. (6)], only a few lowest eigenstates are populated, so the master equation (4) can be solved analytically. This allows us to establish the applicability limits of the phenomenological approach and to calculate the measurement strength  $\lambda$ .

It is convenient to start the analysis from the simple limit, when there is no incident light,  $\mathcal{E} = 0$ . In this case, only the two ground spin states are populated and only the four density matrix elements are nonzero. From Eq. (4) we find that

$$\dot{\rho}_{\uparrow,\uparrow} = \frac{i\Omega_L}{2}(\rho_{\uparrow,\downarrow} - \rho_{\downarrow,\uparrow}), \quad (31a)$$

$$\dot{\rho}_{\uparrow,\downarrow} = \frac{i\Omega_L}{2}(\rho_{\uparrow,\uparrow} - \rho_{\downarrow,\downarrow}). \quad (31b)$$

Here, the two electron spin states with  $S_z = \pm 1/2$  are labeled by the up and down arrows, respectively. The equation for  $\rho_{\downarrow,\uparrow}$  can be obtained from Eq. (31b) by the complex conjugation, and the equation for  $\dot{\rho}_{\downarrow,\downarrow}$  follows from Eq. (31a) and the normalization condition  $\rho_{\uparrow,\uparrow} + \rho_{\downarrow,\downarrow} = 1$ . Both of them can be also obtained from Eqs. (31) by the exchange of  $\uparrow$  and  $\downarrow$ .

The electron spin components are given by

$$S_x = \frac{\rho_{\uparrow,\downarrow} + \rho_{\downarrow,\uparrow}}{2}, \quad S_y = i\frac{\rho_{\uparrow,\downarrow} - \rho_{\downarrow,\uparrow}}{2}, \quad S_z = \frac{\rho_{\uparrow,\uparrow} - \rho_{\downarrow,\downarrow}}{2}. \quad (32)$$

Using Eqs. (31) we arrive at the phenomenological Eqs. (16) with  $\lambda = 0$ , as expected for the case, when the spin is not measured.

Equations (32) are valid for the case of weak excitation also, when the two lowest states are mostly populated. To account for the finite excitation strength we use the perturbation theory and consider  $\Omega_L/\kappa$  and  $\mathcal{E}/\kappa$  as the small parameters. In the zeroth order, only the four density matrix elements discussed above are nonzero and their time derivatives vanish.

In the first order in  $\mathcal{E}/\kappa$  there are another 12 nonzero density matrix elements between the two ground states and the six excited states shown in Fig. 2. They can be found from the equations

$$\begin{aligned} \dot{\rho}_{\downarrow u,\uparrow} &= -i(\omega_0 + g)\rho_{\downarrow u,\uparrow} - \frac{\kappa}{2}(\rho_{\downarrow u,\uparrow} - \rho_{\downarrow l,\uparrow}) \\ &\quad - \frac{\gamma}{2}(\rho_{\downarrow u,\uparrow} + \rho_{\downarrow l,\uparrow}) - \frac{i\mathcal{E}e^{-i\omega t}}{\sqrt{2}}\rho_{\downarrow,\uparrow}, \end{aligned} \quad (33a)$$

$$\begin{aligned} \dot{\rho}_{\downarrow l,\uparrow} &= -i(\omega_0 - g)\rho_{\downarrow l,\uparrow} - \frac{\kappa}{2}(\rho_{\downarrow l,\uparrow} - \rho_{\downarrow u,\uparrow}) \\ &\quad - \frac{\gamma}{2}(\rho_{\downarrow u,\uparrow} + \rho_{\downarrow l,\uparrow}) + \frac{i\mathcal{E}e^{-i\omega t}}{\sqrt{2}}\rho_{\downarrow,\uparrow}, \end{aligned} \quad (33b)$$

$$\dot{\rho}_{\downarrow+,\uparrow} = -i\omega_0\rho_{\downarrow+,\uparrow} - \kappa\rho_{\downarrow+,\uparrow} - \frac{i\mathcal{E}e^{-i\omega t}}{\sqrt{2}}\rho_{\downarrow,\uparrow}. \quad (33c)$$

Another nine equations can be obtained from these three by flipping the spins and by the Hermitian conjugation.

The solution of these equations can be conveniently written using Eqs. (9):

$$\rho_{\downarrow l, \uparrow} = -i\rho_{\downarrow, \uparrow} \frac{\mathcal{E}e^{-i\omega t}}{\sqrt{2}\varkappa} t_1 \left( \frac{g}{\omega - \omega_0 + i\gamma} - 1 \right), \quad (34a)$$

$$\rho_{\downarrow u, \uparrow} = -i\rho_{\downarrow, \uparrow} \frac{\mathcal{E}e^{-i\omega t}}{\sqrt{2}\varkappa} t_1 \left( \frac{g}{\omega - \omega_0 + i\gamma} + 1 \right), \quad (34b)$$

$$\rho_{\downarrow+, \uparrow} = -i \frac{\mathcal{E}}{\varkappa} \rho_{\downarrow, \uparrow} t_0 e^{-i\omega t}. \quad (34c)$$

One can check that the transmission coefficients  $t_0$  and  $t_1$  can be obtained from the density matrix in the first order in  $\mathcal{E}$  from the following relation:

$$\text{Tr}[\rho c_{\pm}] = -i \frac{\mathcal{E}e^{-i\omega t}}{\varkappa} (t_{1,0} \rho_{\uparrow, \uparrow} + t_{0,1} \rho_{\downarrow, \downarrow}). \quad (35)$$

These relations reflect the fact that the transmission coefficient of circularly polarized light is  $t_0$  or  $t_1$  when the helicity of the incident light is opposite or the same as the spin helicity.

The equations of motion for the electron spin can be obtained from the off-diagonal density matrix element between the ground states [see Eqs. (32)]. In the two lowest orders of the perturbation theory we obtain

$$\begin{aligned} \dot{\rho}_{\uparrow, \downarrow} = & \frac{i\Omega_L}{2} (\rho_{\uparrow, \uparrow} - \rho_{\downarrow, \downarrow}) \\ & + \sqrt{2}\varkappa (\rho_{\uparrow u, \downarrow+} + \rho_{\uparrow-, \downarrow u} - \rho_{\uparrow l, \downarrow+} - \rho_{\uparrow-, \downarrow l}) \\ & - \frac{i\mathcal{E}}{\sqrt{2}} [e^{-i\omega t} (\rho_{\uparrow, \downarrow l} - \rho_{\uparrow, \downarrow u} - \sqrt{2}\rho_{\uparrow, \downarrow+}) \\ & + e^{i\omega t} (\rho_{\uparrow u, \downarrow} - \rho_{\uparrow l, \downarrow} + \sqrt{2}\rho_{\uparrow-, \downarrow})]. \end{aligned} \quad (36)$$

Here, the unknown density matrix elements can be found from another two equations in the second order in  $\mathcal{E}/\varkappa$ :

$$\begin{aligned} \dot{\rho}_{\uparrow u, \downarrow+} = & -ig\rho_{\uparrow u, \downarrow+} + i\mathcal{E} \left( e^{i\omega t} \rho_{\uparrow u, \downarrow} - \frac{e^{-i\omega t}}{\sqrt{2}} \rho_{\uparrow, \downarrow+} \right) \\ & - \frac{\gamma}{2} (\rho_{\uparrow u, \downarrow+} + \rho_{\uparrow l, \downarrow+}) - \frac{\varkappa}{2} (3\rho_{\uparrow u, \downarrow+} - \rho_{\uparrow l, \downarrow+}), \end{aligned} \quad (37a)$$

$$\begin{aligned} \dot{\rho}_{\uparrow l, \downarrow+} = & ig\rho_{\uparrow l, \downarrow+} + i\mathcal{E} \left( e^{i\omega t} \rho_{\uparrow l, \downarrow} + \frac{e^{-i\omega t}}{\sqrt{2}} \rho_{\uparrow, \downarrow+} \right) \\ & - \frac{\gamma}{2} (\rho_{\uparrow l, \downarrow+} + \rho_{\uparrow u, \downarrow+}) - \frac{\varkappa}{2} (3\rho_{\uparrow l, \downarrow+} - \rho_{\uparrow u, \downarrow+}). \end{aligned} \quad (37b)$$

Their solution reads

$$\rho_{\uparrow u, \downarrow+} = \frac{\rho_{\uparrow, \downarrow}}{\sqrt{2}} \left( \frac{\mathcal{E}}{\varkappa} \right)^2 \left( \frac{g}{\omega - \omega_0 + i\gamma} + 1 \right) t_0^* t_1, \quad (38a)$$

$$\rho_{\uparrow l, \downarrow+} = \frac{\rho_{\uparrow, \downarrow}}{\sqrt{2}} \left( \frac{\mathcal{E}}{\varkappa} \right)^2 \left( \frac{g}{\omega - \omega_0 + i\gamma} - 1 \right) t_0^* t_1. \quad (38b)$$

Another two density matrix elements in Eq. (36),  $\rho_{\uparrow-, \downarrow u}$  and  $\rho_{\uparrow-, \downarrow l}$ , are obtained from these two by the flip of helicities and the Hermitian conjugation.

Finally, substituting Eqs. (38) and (34) in Eq. (36) we obtain

$$\dot{\rho}_{\uparrow, \downarrow} = \frac{i\Omega_L}{2} (\rho_{\uparrow, \uparrow} - \rho_{\downarrow, \downarrow}) - 2\lambda \rho_{\uparrow, \downarrow}, \quad (39)$$

in agreement with the phenomenological Eqs. (16) for  $S_x$  and  $S_y$ . Here, the measurement strength is given by [61]

$$\lambda = \frac{\mathcal{E}^2}{\varkappa} |t_0 - t_1|^2 \left( 1 + \frac{\gamma[(\omega - \omega_0)^2 + \varkappa^2]}{g^2 \varkappa} \right). \quad (40)$$

This is the main result of this section.

In a similar way one can consider the equation of motion for  $\rho_{\uparrow, \uparrow}$  in the second order of the perturbation theory. In this case the terms with  $\mathcal{E}$  and  $\varkappa$  cancel each other, so one simply obtains

$$\dot{\rho}_{\uparrow, \uparrow} = \frac{i\Omega_L}{2} (\rho_{\uparrow, \downarrow} - \rho_{\downarrow, \uparrow}), \quad (41)$$

which agrees with Eq. (16) for  $S_z$ .

In the absence of trion nonradiative decay,  $\gamma = 0$ , the measurement strength [Eq. (40)] is simply given by

$$\lambda = \frac{\mathcal{E}^2}{\varkappa} |t_0 - t_1|^2. \quad (42)$$

In Fig. 5 we use this relation between  $\lambda$  and  $\mathcal{E}$  along with Eq. (17) to calculate the complex spin precession frequency. One can see that it agrees with the fit of the numerical results. The difference between them is mainly due to the moderate ratio  $\Omega_L/\varkappa = 0.1$ , which is assumed to be very small in the derivation of Eq. (42).

This derivation allows one to control the electron spin precession frequency and relaxation time by intensity and frequency of the external light.

Beyond the limit (6) the excited states should be considerably populated in order to suppress the electron spin precession in the magnetic field. In this case the phenomenological theory breaks down, so the quantum Zeno effect can be described only microscopically taking into account the structure of the optically excited states [41].

Noteworthy, we find that the dependence of  $\lambda$  on  $\omega - \omega_0$  and  $g$  in Eq. (42) reduces to the amplitude transmission coefficients only. This suggests that the measurement strength in this limit can be derived without a detailed analysis of the excited states. This is done in the next section.

#### IV. QUANTUM NONDEMOLITION SPIN MEASUREMENT

Despite the fundamental importance of the quantum Zeno effect, most of its descriptions have a very general form and their validity to every specific system is always questionable [18,62]. Generally, the quantum Zeno effect stems from the interaction of the system with the environment. But in an experimental observation of an effect it is not always clear if the interaction with the environment really represents the measurement that yields the quantum information or not [63]. To demonstrate that the transmission of the light through the cavity truly represents the quantum spin measurement, we discuss it in this section from the perspective of quantum informatics.

In the previous section we demonstrated that the quantum Zeno effect for weak fields is described by Eqs. (16) with the

measurement strength given by Eq. (40). The relaxation of the spin components  $S_x$  and  $S_y$  arises due to the spin measurement backaction. Generally, the relaxation (dephasing) rate of the off-diagonal density matrix element  $\Gamma_{\text{deph}}$  is greater than or equal to the measurement rate  $\Gamma_{\text{meas}}$  [63–65]:

$$\Gamma_{\text{deph}} \geq \Gamma_{\text{meas}}. \quad (43)$$

Note the difference between the measurement rate  $\Gamma_{\text{meas}}$ , which we rigorously define below, and the measurement strength  $\lambda$ , introduced in the previous section. By definition, in the quantum limit the measurement rate equals the dephasing rate.

It is desirable to increase the useful measurement rate while keeping the dephasing rate as low as possible. In optimal conditions one can hope to reach the quantum limit. In this section we identify the conditions when it can be reached for the system under study.

The inequality (43) holds for any external magnetic field while, in particular, for  $\Omega_L = 0$ . In this case, the Hamiltonian  $\mathcal{H}_0$  [Eq. (14)] vanishes and commutes with the observable  $S_z$ , and the relaxation of the spin component  $S_z$  is absent. This means, by definition, the realization of the quantum nondemolition measurement. In this section we consider this limit.

#### A. Optical spin measurement rate

To recall the definition of the measurement rate  $\Gamma_{\text{meas}}$  we assume that the spin is initially prepared in one of the states  $S_z = \pm 1/2$ , e.g., by a short circularly polarized pump pulse [35]. Consequently, the spin orientation can be determined using the continuous probe light, as discussed in Sec. II. In the absence of magnetic field the measurement is quantum nondemolition, so  $S_z$  does not change. After a short measurement time  $t$ , after a few photons are detected, one cannot say for sure what is the electron spin state, but one can calculate the two conditional probabilities  $P_{\pm}(t)$  for the spin-up and spin-down states, respectively.

The quantum statistical average

$$\mathcal{I}(t) = - \sum_{\pm} \overline{P_{\pm}(t) \ln[P_{\pm}(t)]} \quad (44)$$

yields the ‘‘entropy,’’ which characterizes our knowledge about the spin direction. Note that  $\mathcal{I}(t)$  does not describe the real entropy of the system, which is zero, because the electron is actually completely spin polarized. The measurement rate is defined by

$$\Gamma_{\text{meas}} = -\dot{\mathcal{I}}(0), \quad (45)$$

and represents the ‘‘entropy’’ decrease rate at the beginning of the spin measurement.

In the previous section we considered the spin measurement by the detection of the intensities of  $\sigma^+$  and  $\sigma^-$  polarized components of the transmitted light. Their dependence on the spin direction [Eq. (10)] allows one to deduce the spin direction from the circular polarization of the transmitted light. Generally, the polarization of the light is described by the vectors of the Stokes parameters  $\xi_{\pm}$  for the cases of spin-up and spin-down electrons, respectively [37,66].

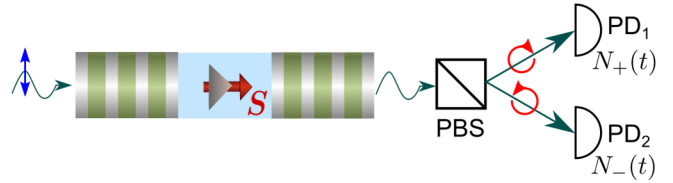


FIG. 6. Scheme of the quantum nondemolition spin measurement by linearly polarized light. The magnetic field is absent. The transmitted light is separated into two orthogonally polarized components by the polarizing beam splitter (PBS), and then the photons in the two polarizations are independently counted using the photodetectors (PDs).

The amplitude transmission coefficients of  $\sigma^{\pm}$  light are given similarly to Eq. (10) by

$$t_{\pm} = \frac{t_0 + t_1}{2} \pm (t_1 - t_0)S_z \quad (46)$$

[see also Eqs. (35)]. In the canonical basis [67] the circular components of the electric field are given by  $E_{\pm} = (\mp E_x + iE_y)/\sqrt{2}$ , so the Stokes parameters can be expressed as

$$\begin{aligned} \xi_{1,\pm} &= \pm \frac{2\text{Im}(t_1 t_0^*)}{|t_1^2| + |t_0^2|}, & \xi_{2,\pm} &= \pm \frac{|t_1^2| - |t_0^2|}{|t_1^2| + |t_0^2|}, \\ \xi_{3,\pm} &= - \frac{2\text{Re}(t_1 t_0^*)}{|t_1^2| + |t_0^2|}. \end{aligned} \quad (47)$$

Thus, the spin polarization can be measured using both the Faraday rotation and the ellipticity of the transmitted light, which are proportional to  $\xi_1$  and  $\xi_2$ , respectively. To determine one of them, the light transmitted through the cavity can be analyzed using the polarizing beam splitter and two photodetectors, as shown in Fig. 6. Note that the total intensity of the transmitted light being proportional to  $T_+ + T_-$  is independent of  $S_z$  [see Eq. (10)].

To maximize the detection sensitivity one can adjust the polarizations separated by the beam splitter to measure a combination of the Faraday rotation and ellipticity signals. Generally, by the appropriate rotation of the polarization basis of the Poincaré sphere one can obtain the Stokes parameters of the form

$$\xi_{1',\pm} = 0, \quad \xi_{2',\pm} = \pm \xi, \quad \xi_{3',+} = \xi_{3',-}. \quad (48)$$

Here, the primes denote the rotated axes. In this basis the spin state is distinguished by the second Stokes parameter only, which is the circular polarization degree. From Eqs. (47) one can see that

$$\xi = \sqrt{\xi_{1,\pm}^2 + \xi_{2,\pm}^2} = \frac{|t_1^2 - t_0^2|}{|t_1^2| + |t_0^2|}. \quad (49)$$

As expected, the Stokes parameters are different only if the transmission coefficients  $t_0$  and  $t_1$  are different.

In what follows we assume that  $\xi_{2'}$  is measured as shown in Fig. 6. We denote the numbers of the detected circularly polarized photons after the measurement time  $t$  as  $N_{\pm}(t)$  (see Fig. 6). If they are large, the Stokes parameter is given by

$$\xi_{2'} = \frac{N_+ - N_-}{N_+ + N_-} = \pm \xi. \quad (50)$$

However, if  $N_{\pm}$  are small, this equation yields only an estimate for  $\xi_{2\pm}$ , which is a random number and can differ from  $\pm\xi$ .

### B. Entanglement between electron and photon

The spin measurement through the photon detection can be viewed as a result of the entanglement between electron and photon spins [68–70]. The electron and photon represent in this case the two qubits. The photon detection destroys the entanglement, which leads to the dephasing of the electron spin. The frequent photon detection leads to the quick relaxation of the off-diagonal spin density matrix elements, which causes the quantum Zeno effect. So the measurement strength is determined by the degree of the spin-photon entanglement.

To put it on a quantitative basis, we write down the two-particle wave function of an electron and a single transmitted photon:

$$|\Psi_{e-ph}\rangle = \frac{(\chi_+ t_1, \chi_+ t_0, \chi_- t_0, \chi_- t_1)}{\sqrt{|t_1^2| + |t_0^2|}}. \quad (51)$$

Here, we use the basis states  $|\uparrow, \sigma^+\rangle$ ,  $|\uparrow, \sigma^-\rangle$ ,  $|\downarrow, \sigma^+\rangle$ ,  $|\downarrow, \sigma^-\rangle$ , with an arrow denoting the electron spin state and  $\sigma^{\pm}$  denoting the photon polarization. The components of the electron spinor are denoted as  $\chi_{\pm}$ . Equation (51) represents a pure state, so its concurrence is given by [71]

$$C = |\langle\Psi_{e-ph}|\mathcal{T}|\Psi_{e-ph}\rangle|, \quad (52)$$

where  $\mathcal{T}$  denotes the time inversion (multiplication by the second Pauli matrices of both qubits and complex conjugation). The straightforward calculation yields

$$C = 2\xi|S_x + iS_y|. \quad (53)$$

This establishes the relation between the concurrence and the difference of the Stokes parameters  $\xi_{2,\pm}$ . The spin components  $S_x$  and  $S_y$  in Eq. (53) reflect the fact that the destruction of the entanglement leads to the relaxation of the off-diagonal density matrix elements [see Eqs. (15) and (16)].

### C. Calculation of the measurement rate

To calculate the measurement rate we consider a short measurement time  $t$ , when the average number of the detected photons  $\overline{N(t)} = \overline{N_+(t)} + \overline{N_-(t)}$  is small:  $\overline{N(t)} \ll 1$ . In this case, we can neglect the probability to detect two photons and consider zero or one detected photon only.

In the case of  $N_+ = 1$  and  $N_- = 0$ , the conditional probabilities of spin-up and spin-down states are given by

$$P_{\pm} = \frac{1 \pm \xi}{2} \quad (54)$$

[see Eq. (50)]. In the case of  $N_+ = 0$ ,  $N_- = 1$ , the  $\pm$  sign on the right-hand side should be flipped, and in the trivial case of  $N_+ = N_- = 0$  one has  $P_{\pm} = 1/2$ , since there is no ground for the spin direction estimation.

As an example, if  $\xi = 1$ , then the transmitted light is always circularly polarized and its polarization is  $\sigma^{\pm}$  (in the rotated basis) for  $S_z = \pm 1/2$ , respectively. In this case, a single photon detection strictly yields the electron spin orientation: Either  $P_+$  or  $P_-$  is equal to unity as follows from Eq. (54).

In the opposite limit of  $\xi \ll 1$ , the polarizations of the transmitted light for  $S_z = \pm 1/2$  are very similar, and after a single photon detection  $P_{\pm} \approx 1/2$  in Eq. (54), so it is difficult to say what is the actual electron spin state.

Generally, Eq. (54) along with the definition (44) yields

$$\mathcal{I}(t) = \ln(2) - \overline{N(t)} \left[ \frac{1+\xi}{2} \ln(1+\xi) + \frac{1-\xi}{2} \ln(1-\xi) \right]. \quad (55)$$

This leads to the measurement rate [Eq. (45)]

$$\Gamma_{\text{meas}} = \left[ \frac{1+\xi}{2} \ln(1+\xi) + \frac{1-\xi}{2} \ln(1-\xi) \right] \overline{N}, \quad (56)$$

where  $\overline{N}$  is the average flux of the transmitted photons. This expression is general. It is valid for arbitrary  $\xi$  and can be used to calculate the measurement rate for any optical spin measurement.

The photon flux is given by

$$\overline{N} = 2\kappa_2 \langle c_+^\dagger c_+ + c_-^\dagger c_- \rangle, \quad (57)$$

where we recall that  $\kappa_2$  is the photon amplitude decay rate through the right mirror of the cavity (the light is assumed to be incident at the left one). Making use of the steady state density matrix found in Sec. III C, we obtain

$$\overline{N} = 2\kappa_2 \frac{\mathcal{E}^2}{\kappa^2} (|t_0^2| + |t_1^2|). \quad (58)$$

Now the substitution of this expression along with Eq. (49) in Eq. (56) yields the spin measurement rate  $\Gamma_{\text{meas}}$ .

It should be compared with the dephasing rate, i.e., the rate of the decay of the off-diagonal spin density matrix element:

$$\Gamma_{\text{deph}} = 2\lambda \quad (59)$$

[see Eqs. (16) and (32)]. Here,  $\lambda$  is given by Eq. (40).

In Fig. 7(a) we compare the spin measurement and dephasing rates as functions of the probe frequency. Both rates show the three peaks at the same frequencies as the transmission coefficient: bare cavity and polariton frequencies. One can see that the dephasing rate is always larger than the measurement rate, so the inequality (43) is satisfied.

The trion decay with the rate  $\gamma$  increases the dephasing rate in Eq. (40), so in Fig. 7 we consider the limit  $\gamma = 0$ . Moreover, it follows from Eq. (58) that the detected photon flux is proportional to the ratio  $\kappa_2/\kappa$ , so the more photons escape the cavity through the right mirror, the higher is the measurement rate. The blue dotted and red dashed curves demonstrate that the measurement rate is two times larger in the limit  $\kappa_2 \rightarrow \kappa$  than in the case of a symmetric cavity,  $\kappa_2 = \kappa/2$ . However, even if all the photons escape the cavity through the right mirror and are captured by the photodetectors, the measurement rate is still considerably smaller than the dephasing rate, as shown in Fig. 7(b).

The measurement rate approaches the dephasing rate for strongly detuned light, because the measurement in this case becomes almost nonperturbing. However, below we will show that the measurement rate can be increased up to the dephasing rate at all probe frequencies.

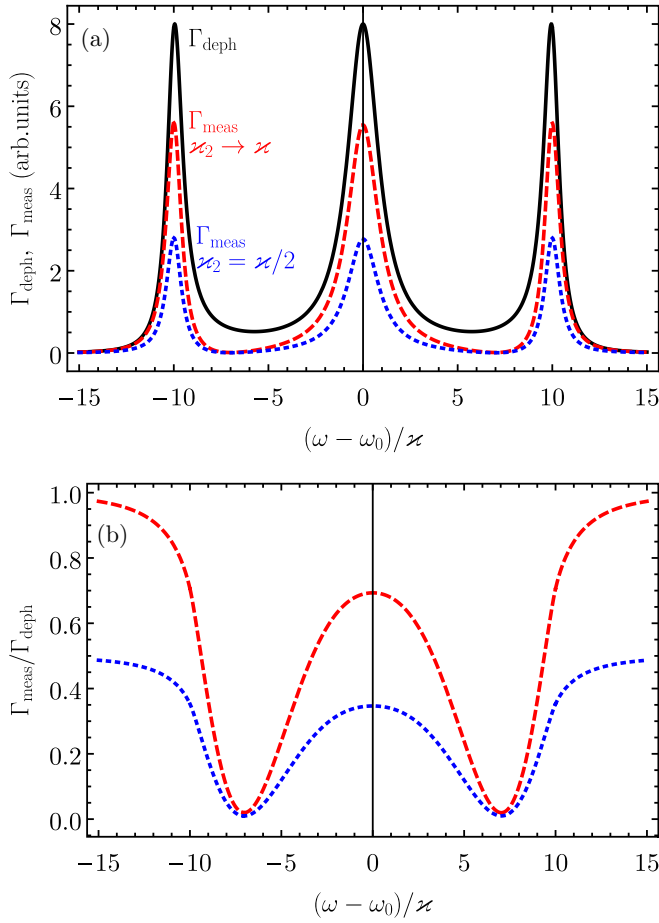


FIG. 7. (a) Spin measurement and dephasing rates, calculated after Eqs. (56) (red dashed and blue dotted curves) and (59) (black solid curve), respectively, for  $\gamma = 0$  and  $g/\chi = 10$ . For the blue dotted and red dashed curves,  $\varkappa_2 = \varkappa/2$  and  $\varkappa_2 \rightarrow \varkappa$ , respectively. (b) Ratio of the measurement and dephasing rates for the same parameters shown with the same colors.

#### D. Reaching the quantum limit

To summarize the previous section, the optimization of the structure parameters  $\gamma = 0$  and  $\varkappa_2 \rightarrow \varkappa$  does not allow one to reach the quantum limit. This can be explained using the expression for the difference of the Stokes parameters (49). For example, if  $t_0 = 1$  and  $t_1 = -1$ , then the transmitted light is always polarized linearly perpendicular to the polarization of the incident light. The Stokes parameters are the same for spin-up and spin-down electrons, so the detection scheme shown in Fig. 6 does not allow one to determine the electron spin state. However, the phase of the transmitted light is opposite for the two spin states. This phase can be measured using the homodyne detection. The homodyne detection is often used to reach the quantum limit [63], but to date it was not clear how it changes the measurement rate.

In the homodyne detection scheme (Fig. 8), the light emitted from the cavity interferes with the field of the local oscillator, which has a fixed phase relative to the light incident at the cavity. The total amplitudes of the circularly polarized components of light before the polarizing beam splitter have

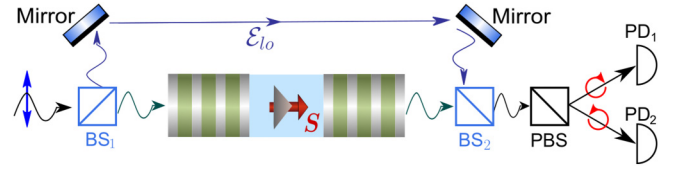


FIG. 8. Scheme of the homodyne nondemolition spin measurement. Linearly polarized light is separated into two beams by the beam splitter BS<sub>1</sub>. After one of them passes through the cavity, they are mixed by the beam splitter BS<sub>2</sub>. The photon counting scheme is the same as in Fig. 6.

the form

$$E_{\pm} \propto t_{\pm} \mathcal{E} + \mathcal{E}_{l_0}, \quad (60)$$

where  $\mathcal{E}_{l_0}$  is proportional to the amplitude of the local oscillator field (the effective decrease of the transmission coefficients  $t_{\pm}$  due to the beam splitter BS<sub>2</sub> in Fig. 8 can be accounted for by the renormalization of  $\mathcal{E}_{l_0}$ ). In this case, the above theory is valid provided the effective transmission coefficients

$$\tilde{t}_{\pm} = t_{\pm} + t_{l_0} \quad (61)$$

are used instead of  $t_{\pm}$  with  $t_{l_0} = \mathcal{E}_{l_0}/\mathcal{E}$ . For the large amplitude of the local oscillator,  $t_{l_0} \gg 1$ , the difference between the Stokes parameters is small,

$$\xi = \frac{|t_1 - t_0|}{|t_0|} \ll 1, \quad (62)$$

so the measurement rate Eq. (56) can be written as

$$\Gamma_{\text{meas}} = \frac{\xi^2 \bar{N}}{2}. \quad (63)$$

However, the photon flux is  $2|t_{l_0}^2|/(|t_1^2| + |t_0^2|)$  times larger than without the homodyne detection [Eq. (58)]. So the total measurement rate for the homodyne detection is

$$\Gamma_{\text{meas}}^{\text{homo}} = 2|t_1 - t_0|^2 \varkappa_2 \frac{\mathcal{E}^2}{\varkappa^2}. \quad (64)$$

From a comparison with Eqs. (59) and (40) one can see that for  $\gamma = 0$  and  $\varkappa_2 = \varkappa$  the quantum limit is reached at all frequencies of the probe light.

#### V. SPIN STATISTICS

The electron spin measurement unavoidably leads to the quantum Zeno effect and modifies the whole electron spin statistics. In this section we return to the case when an external transverse magnetic field is applied to the system. Vanishing of the spin precession frequency with an increase of the measurement strength shown in Fig. 5 evidences the qualitative change of the regime of the spin dynamics.

One can argue that the qualitative change of the spin dynamics is a signature of a quantum dynamical phase transition [57]. However, the simple vanishing of the precession frequency due to the quantum Zeno effect is similar to the classical overdamped oscillator. To prove the quantum nature of the spin noise, in this section we calculate the fourth-order spin noise spectrum, which would be zero for any classical noise.

In the system under study the third-order correlator vanishes, because the spin is zero on average. Generally, to describe the nontrivial contribution to the fourth-order correlation function, the cumulant is introduced [44] according to

$$\begin{aligned} C_4(\tau_1, \tau_2, \tau_3) &= \langle S_z(0)S_z(\tau_1)S_z(\tau_2)S_z(\tau_3) \rangle \\ &\quad - \langle S_z(0)S_z(\tau_1) \rangle \langle S_z(\tau_2)S_z(\tau_3) \rangle \\ &\quad - \langle S_z(0)S_z(\tau_2) \rangle \langle S_z(\tau_1)S_z(\tau_3) \rangle \\ &\quad - \langle S_z(0)S_z(\tau_3) \rangle \langle S_z(\tau_1)S_z(\tau_2) \rangle. \end{aligned} \quad (65)$$

For classical Gaussian noise the cumulants beyond the second order are zero. Here, for a single spin, the nonzero fourth-order cumulant stems from the ‘‘quantum nature’’ of the spin: It takes only one of the two eigenvalues  $S_z = \pm 1/2$  at the four moments 0,  $\tau_1$ ,  $\tau_2$ , and  $\tau_3$  [72]. Usually, the fourth-order spin correlation function is hardly accessible experimentally [73], but in the system under study it can be easily determined from the photon counting statistics, as described in Sec. II for the second-order correlation function.

Higher-order spin correlators can be calculated, for example, using the path integrals [55,72] or Ito calculus [74,75]. We use the formalism of the Kraus operators introduced in Sec. III A. In analogy with Eq. (22), the fourth-order spin correlator is given by the integral over  $s_1, s_2, s_3$ , and  $s_4$ , which correspond to the measurements at the four time moments  $t = 0, \tau_1, \tau_2$ , and  $\tau_3$ . The straightforward calculation shows that the high-order correlators for a single electron spin reduce to the products of the second-order correlators at the consecutive time moments. Thus, for  $0 < \tau_1 < \tau_2 < \tau_3$ , the first two terms in Eq. (65) cancel each other and we obtain

$$\begin{aligned} C_4(\tau_1, \tau_2, \tau_3) &= -\langle S_z(0)S_z(\tau_2) \rangle \langle S_z(\tau_1)S_z(\tau_3) \rangle \\ &\quad - \langle S_z(0)S_z(\tau_3) \rangle \langle S_z(\tau_1)S_z(\tau_2) \rangle. \end{aligned} \quad (66)$$

This allows us to calculate the fourth-order spin correlation function using Eq. (23).

The fourth-order correlator depends on the three time intervals, and its Fourier transform depends on the three frequencies. For simplicity, it is often reduced to the bispectrum which is given by

$$B(\omega_1, \omega_2) = \iint d\tau_1 d\tau_2 d\tau e^{i\omega_1\tau_1 + i\omega_2\tau_2} C_4(\tau_1, \tau, \tau + \tau_2). \quad (67)$$

Qualitatively it reflects the degree of the correlation between the spin noise at frequencies  $\omega_1$  and  $\omega_2$ .

The modification of the bispectrum with an increase of the measurement strength is shown in Fig. 9. Note that the vertical axis goes from top to bottom, so the bispectrum is mostly negative. It is always an even function of  $\omega_1$  and  $\omega_2$ .

Under the weak measurement,  $\lambda \ll \Omega_L$  [Fig. 9(a)], the bispectrum consists of four peaks at the frequencies  $\omega_{1,2} = \pm\Omega_L$ . For the positive frequencies the bispectrum has the form

$$B(\omega_1, \omega_2) = \frac{\lambda[(\delta_1 + \delta_2)^2 + 4\lambda^2](\delta_1\delta_2 - \lambda^2)}{16(\lambda^2 + \delta_1^2)^2(\lambda^2 + \delta_2^2)^2}, \quad (68)$$

where  $\delta_{1,2} = \omega_{1,2} - \Omega_L$ .

With an increase of the measurement strength the peaks become broader and shift to the lower frequencies along the

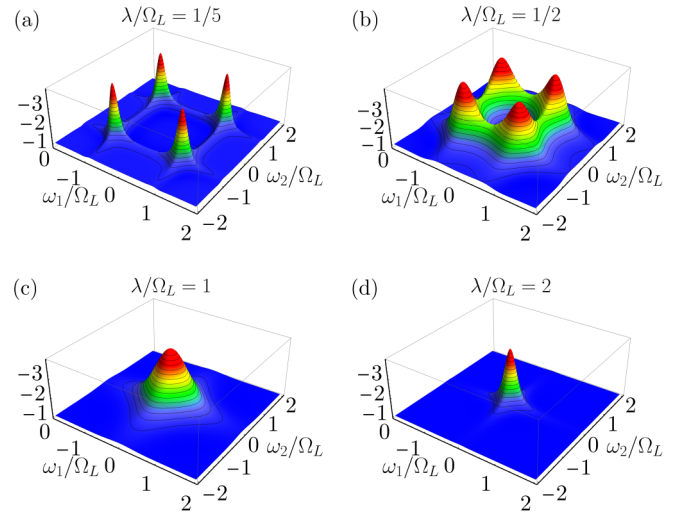


FIG. 9. Spin noise bispectrum  $B(\omega_1, \omega_2)$  in arbitrary units calculated after Eq. (66) for the different measurement strengths given in the labels.

$|\omega_1| = |\omega_2|$  directions. The peaks start to overlap as shown in Fig. 9(b) and eventually merge at  $\omega_1 = \omega_2 = 0$  at the phase transition,  $\lambda = \Omega_L$  [Fig. 9(c)]. Note that there is no abrupt change in the bispectrum as in the case of the second-order phase transition described by the continuously changing order parameter.

Under the strong spin measurement  $\lambda \gg \Omega_L$  the spin noise bispectrum has the form

$$B(\omega_1, \omega_2) = \frac{\gamma}{2} \frac{\omega_1^2 \omega_2^2 - \gamma^2(\omega_1^2 + \omega_2^2) - 3\gamma^4}{(\omega_1^2 + \gamma^2)^2(\omega_2^2 + \gamma^2)^2}, \quad (69)$$

where  $\gamma = \Omega_L^2/(2\lambda)$  is the spin relaxation rate in this limit [see Eq. (17)]. This expression coincides with the bispectrum of the telegraph noise [72]. Thus when the quantum Zeno effect is strong, the electron spin is in every time moment either  $+1/2$  or  $-1/2$ , as required for the telegraph noise.

## VI. DISCUSSION AND CONCLUSION

Generally, the spin measurement leads to anisotropic spin relaxation. In order to reach the quantum limit this should be the only source of spin relaxation, while there are many other additional spin relaxation mechanisms of an electron in a QD. In a weak magnetic field, the dominant spin relaxation mechanisms are the hyperfine interaction [43] and Auger trion recombination [76], which lead to the spin relaxation on the timescale from a few nanoseconds to tens of microseconds. In the same time, the characteristic timescale  $1/\varkappa$  is usually of the order of 1 ps, so there is a time gap of at least three orders when the spin relaxation can be neglected. The model of the quantum Zeno effect developed in this paper is valid in this case. In particular, for zero magnetic field, the nondemolition spin measurement can be realized and the quantum limit can be reached using the homodyne detection.

The calculations in this work were done for a particular choice of the spin photon interface. However, we believe that they give an essential physical insight and

can be adapted to other situations such as weak coupling regime, different polarization configurations, different geometries including photonic crystals, waveguides, and plasmonic structures [77–84], and different material systems including trapped atoms, color centers, and rare earth ions.

The ratio of the measurement and dephasing rates was not studied for most of the particular realizations of the spin-photon interfaces [32,35,85,86]. However, from our analysis we can expect that it is very small (far from the quantum limit) for the QD systems in the weak coupling regime [87–89], because most of the emitted photons are not detected in this case. The situation may change in the case of the resonance fluorescence measurements [90–93], but this requires a spin measurement by many photons. In the system under study the spin measurement can be performed in principle by a single photon [32,35].

To summarize, we have developed a microscopic theory of the quantum Zeno effect for a continuous measurement of a single electron spin noise in a QD micropillar cavity. We showed that in the limit of a small population of trion states, the suppression of the spin precession in a magnetic field is described by a single parameter, the measurement strength given by Eq. (40). We demonstrated that the quantum Zeno effect results from the destruction of the entanglement

between the electron spin and photon polarizations. We derived the general expression for the optical spin measurement rate analyzing the Stokes parameters of the transmitted light [Eq. (56)]. We demonstrated that the high-order spin statistics qualitatively change at the transition between the regime of quantum coherent dynamics and the quantum Zeno phase. They agree with the telegraph noise for the strong continuous spin measurement. Finally, we demonstrated that the quantum limit can be reached for any probe frequency using a one-sided cavity and the homodyne nondemolition spin measurement.

The developed theory allows one to tune the strength of the measurement backaction and to maximize the quantum information gain rate for the given spin dephasing rate.

## ACKNOWLEDGMENTS

We gratefully acknowledge fruitful discussions with A. N. Poddubny and the partial financial support by the RF President Grant No. MK-1576.2019.2 and the Foundation for the Advancement of Theoretical Physics and Mathematics “BASIS.” The numerical calculations by N.V.L. were supported by the Russian Science Foundation Grant No. 19-12-00051. The analytical calculations by D.S.S. were supported by the Russian Science Foundation Grant No. 19-72-00081.

- 
- [1] L. A. Khal'fin, Contribution to the decay theory of a quasi-stationary state, *Sov. Phys. JETP* **6**, 1053 (1958).
  - [2] P. Facchi and S. Pascazio, Quantum Zeno dynamics: Mathematical and physical aspects, *J. Phys. A: Math. Theor.* **41**, 493001 (2008).
  - [3] R. P. Hardie and R. K. Gaye, *Physica* by Aristotle (translation), in *The Works of Aristotle*, edited by J. A. Smith and W. D. Ross (Clarendon Press, Oxford, 1930), Vol. II.
  - [4] B. Misra and E. C. G. Sudarshan, The Zeno's paradox in quantum theory, *J. Math. Phys.* **18**, 756 (1977).
  - [5] D. Guéry-Odelin, A. Ruschhaupt, A. Kiely, E. Torrontegui, S. Martínez-Garaot, and J. G. Muga, Shortcuts to adiabaticity: Concepts, methods, and applications, *Rev. Mod. Phys.* **91**, 045001 (2019).
  - [6] L. Pezzè, A. Smerzi, M. K. Oberthaler, R. Schmied, and P. Treutlein, Quantum metrology with nonclassical states of atomic ensembles, *Rev. Mod. Phys.* **90**, 035005 (2018).
  - [7] J. A. Gross, C. M. Caves, G. J. Milburn, and J. Combes, Qubit models of weak continuous measurements: Markovian conditional and open-system dynamics, *Quantum Sci. Technol.* **3**, 024005 (2018).
  - [8] A. G. Kofman and G. Kurizki, Acceleration of quantum decay processes by frequent observations, *Nature (London)* **405**, 546 (2000).
  - [9] P. Facchi, H. Nakazato, and S. Pascazio, From the Quantum Zeno to the Inverse Quantum Zeno Effect, *Phys. Rev. Lett.* **86**, 2699 (2001).
  - [10] D. E. Chang, J. S. Douglas, A. González-Tudela, C.-L. Hung, and H. J. Kimble, Colloquium: Quantum matter built from nanoscopic lattices of atoms and photons, *Rev. Mod. Phys.* **90**, 031002 (2018).
  - [11] D. Leibfried, R. Blatt, C. Monroe, and D. Wineland, Quantum dynamics of single trapped ions, *Rev. Mod. Phys.* **75**, 281 (2003).
  - [12] J. Wolters, M. Strauß, R. S. Schoenfeld, and O. Benson, Quantum Zeno phenomenon on a single solid-state spin, *Phys. Rev. A* **88**, 020101(R) (2013).
  - [13] D. Sokolovski and E. Ya. Sherman, Spin measurements and control of cold atoms using spin-orbit fields, *Phys. Rev. A* **89**, 043614 (2014).
  - [14] N. Kalb, J. Cramer, D. J. Twitchen, M. Markham, R. Hanson, and T. H. Tamirniau, Experimental creation of quantum Zeno subspaces by repeated multi-spin projections in diamond, *Nat. Commun.* **7**, 13111 (2016).
  - [15] M. Pfender, P. Wang, H. Sumiya, S. Onoda, W. Yang, D. B. R. Dasari, P. Neumann, X.-Y. Pan, J. Isoya, R.-B. Liu, and J. Wrachtrup, High-resolution spectroscopy of single nuclear spins via sequential weak measurements, *Nat. Commun.* **10**, 594 (2019).
  - [16] K. S. Cujia, J. M. Boss, K. Herb, J. Zopes, and C. L. Degen, Tracking the precession of single nuclear spins by weak measurements, *Nature (London)* **571**, 230 (2019).
  - [17] D. Klauser, W. A. Coish, and D. Loss, Nuclear spin dynamics and Zeno effect in quantum dots and defect centers, *Phys. Rev. B* **78**, 205301 (2008).
  - [18] T. Nutz, P. Androvitsaneas, A. Young, R. Oulton, and D. P. S. McCutcheon, Stabilization of an optical transition energy via nuclear Zeno dynamics in quantum-dot-cavity systems, *Phys. Rev. A* **99**, 053853 (2019).
  - [19] O. Hosten, M. T. Rakher, J. T. Barreiro, N. A. Peters, and P. G. Kwiat, Counterfactual quantum computation through quantum interrogation, *Nature (London)* **439**, 949 (2006).

- [20] G. Gordon and G. Kurizki, Preventing Multipartite Disentanglement by Local Modulations, *Phys. Rev. Lett.* **97**, 110503 (2006).
- [21] A. Signoles, A. Facon, D. Grosso, I. Dotsenko, S. Haroche, J.-M. Raimond, M. Brune, and S. Gleyzes, Confined quantum Zeno dynamics of a watched atomic arrow, *Nat. Phys.* **10**, 715 (2014).
- [22] F. Schäfer, I. Herrera, S. Cherukattil, C. Lovecchio, F. S. Cataliotti, F. Caruso, and A. Smerzi, Experimental realization of quantum Zeno dynamics, *Nat. Commun.* **5**, 3194 (2014).
- [23] F. Piacentini, A. Avella, E. Rebufello, R. Lussana, F. Villa, A. Tosi, M. Gramegna, G. Brida, E. Cohen, L. Vaidman, I. P. Degiovanni, and M. Genovese, Determining the quantum expectation value by measuring a single photon, *Nat. Phys.* **13**, 1191 (2017).
- [24] G. A. Paz-Silva, A. T. Rezakhani, J. M. Dominy, and D. A. Lidar, Zeno Effect for Quantum Computation and Control, *Phys. Rev. Lett.* **108**, 080501 (2012).
- [25] J. Stolze, D. Suter, and D. P. Divincenzo, *Quantum Computing: A Short Course from Theory to Experiment* (Wiley-VCH, Berlin, 2008).
- [26] D. V. Khomitsky, L. V. Gulyaev, and E. Ya. Sherman, Spin dynamics in a strongly driven system: Very slow Rabi oscillations, *Phys. Rev. B* **85**, 125312 (2012).
- [27] R. Raussendorf and H. J. Briegel, A One-Way Quantum Computer, *Phys. Rev. Lett.* **86**, 5188 (2001).
- [28] K. Koshino, S. Ishizaka, and Y. Nakamura, Deterministic photon-photon  $\sqrt{\text{swap}}$  gate using a  $\Lambda$  system, *Phys. Rev. A* **82**, 010301(R) (2010).
- [29] S. Rosenblum, S. Parkins, and B. Dayan, Photon routing in cavity QED: Beyond the fundamental limit of photon blockade, *Phys. Rev. A* **84**, 033854 (2011).
- [30] I. Shomroni, S. Rosenblum, Y. Lovsky, O. Bechler, G. Guendelman, and B. Dayan, All-optical routing of single photons by a one-atom switch controlled by a single photon, *Science* **345**, 903 (2014).
- [31] I. Schwartz, D. Cogan, E. R. Schmidgall, Y. Don, L. Gantz, O. Kenneth, N. H. Lindner, and D. Gershoni, Deterministic generation of a cluster state of entangled photons, *Science* **354**, 434 (2016).
- [32] D. S. Smirnov, B. Reznichenko, A. Auffèves, and L. Lanco, Measurement back action and spin noise spectroscopy in a charged cavity QED device in the strong coupling regime, *Phys. Rev. B* **96**, 165308 (2017).
- [33] A. Kavokin, J. J. Baumberg, G. Malpuech, and F. P. Laussy, *Microcavities* (Oxford University Press, Oxford, UK, 2007).
- [34] D. Najer, I. Söllner, P. Sekatski, V. Dolique, M. C. Löbl, D. Riedel, R. Schott, S. Starosielec, S. R. Valentin, A. D. Wieck, N. Sangouard, A. Ludwig, and R. J. Warburton, A gated quantum dot strongly coupled to an optical microcavity, *Nature (London)* **575**, 622 (2019).
- [35] D. S. Smirnov, M. M. Glazov, E. L. Ivchenko, and L. Lanco, Theory of optical spin control in quantum dot microcavities, *Phys. Rev. B* **92**, 115305 (2015).
- [36] C. Arnold, J. Demory, V. Loo, A. Lemaitre, I. Sagnes, M. Glazov, O. Krebs, P. Voisin, P. Senellart, and L. Lanco, Macroscopic rotation of photon polarization induced by a single spin, *Nat. Commun.* **6**, 6236 (2015).
- [37] E. L. Ivchenko, *Optical Spectroscopy of Semiconductor Nanostructures* (Alpha Science, Harrow, UK, 2005).
- [38] D. F. Walls and G. J. Milburn, *Quantum Optics* (Springer, New York, 2007).
- [39] X. Marie, T. Amand, P. Le Jeune, M. Paillard, P. Renucci, L. E. Golub, V. D. Dymnikov, and E. L. Ivchenko, Hole spin quantum beats in quantum-well structures, *Phys. Rev. B* **60**, 5811 (1999).
- [40] H. Carmichael, *An Open System Approach to Quantum Optics* (Springer, Berlin, 1993).
- [41] S. V. Poltavtsev, I. I. Ryzhov, M. M. Glazov, G. G. Kozlov, V. S. Zapasskii, A. V. Kavokin, P. G. Lagoudakis, D. S. Smirnov, and E. L. Ivchenko, Spin noise spectroscopy of a single quantum well microcavity, *Phys. Rev. B* **89**, 081304(R) (2014).
- [42] C. Y. Hu, A. Young, J. L. O'Brien, W. J. Munro, and J. G. Rarity, Giant optical Faraday rotation induced by a single-electron spin in a quantum dot: Applications to entangling remote spins via a single photon, *Phys. Rev. B* **78**, 085307 (2008).
- [43] M. M. Glazov, *Electron and Nuclear Spin Dynamics in Semiconductor Nanostructures* (Oxford University Press, Oxford, UK, 2018).
- [44] D. S. Smirnov, V. N. Mantsevich, and M. M. Glazov, Theory of optically detected spin noise in nanosystems, *Phys. Usp.*, (2021).
- [45] L. D. Landau and E. M. Lifshitz, *Statistical Physics, Part 1* (Butterworth-Heinemann, Oxford, UK, 2000).
- [46] C. M. Caves and G. J. Milburn, Quantum-mechanical model for continuous position measurements, *Phys. Rev. A* **36**, 5543 (1987).
- [47] C. Presilla, R. Onofrio, and U. Tambini, Measurement quantum mechanics and experiments on quantum Zeno effect, *Ann. Phys.* **248**, 95 (1996).
- [48] B. J. Sussman, Five ways to the nonresonant dynamic Stark effect, *Am. J. Phys.* **79**, 477 (2011).
- [49] I. I. Ryzhov, G. G. Kozlov, D. S. Smirnov, M. M. Glazov, Y. P. Efimov, S. A. Eliseev, V. A. Lovtcius, V. V. Petrov, K. V. Kavokin, A. V. Kavokin, and V. S. Zapasskii, Spin noise explores local magnetic fields in a semiconductor, *Sci. Rep.* **6**, 21062 (2016).
- [50] A. G. Kofman and G. Kurizki, Quantum Zeno effect on atomic excitation decay in resonators, *Phys. Rev. A* **54**, R3750(R) (1996).
- [51] A. G. Kofman, G. Kurizki, and T. Opatrny, Zeno and anti-Zeno effects for photon polarization dephasing, *Phys. Rev. A* **63**, 042108 (2001).
- [52] D. Sokolovski and E. Ya. Sherman, Measurement of noncommuting spin components using spin-orbit interaction, *Phys. Rev. A* **84**, 030101(R) (2011).
- [53] E. Ya. Sherman and D. Sokolovski, von Neumann spin measurements with Rashba fields, *New J. Phys.* **16**, 015013 (2014).
- [54] K. Kraus, Measuring processes in quantum mechanics I. Continuous observation and the watchdog effect, *Found. Phys.* **11**, 547 (1981).
- [55] A. Bednorz, W. Belzig, and A. Nitzan, Nonclassical time correlation functions in continuous quantum measurement, *New J. Phys.* **14**, 013009 (2012).
- [56] R.-B. Liu, S.-H. Fung, H.-K. Fung, A. N. Korotkov, and L. J. Sham, Dynamics revealed by correlations of time-distributed

- weak measurements of a single spin, *New J. Phys.* **12**, 013018 (2010).
- [57] G. A. Álvarez, E. P. Danieli, P. R. Levstein, and H. M. Pastawski, Environmentally induced quantum dynamical phase transition in the spin swapping operation, *J. Chem. Phys.* **124**, 194507 (2006).
- [58] F. Li, J. Ren, and N. A. Sinitsyn, Quantum Zeno effect as a topological phase transition in full counting statistics and spin noise spectroscopy, *Europhys. Lett.* **105**, 27001 (2014).
- [59] J. Ren and N. A. Sinitsyn, Braid group and topological phase transitions in nonequilibrium stochastic dynamics, *Phys. Rev. E* **87**, 050101(R) (2013).
- [60] K. Snizhko, P. Kumar, and A. Romito, Quantum Zeno effect appears in stages, *Phys. Rev. Research* **2**, 033512 (2020).
- [61] It can be also compactly written as  $\lambda = (\mathcal{E}^2/\varkappa)\text{Re}(t_0 + t_1 - 2t_0t_1^*)$ .
- [62] T. Petrosky, S. Tasaki, and I. Prigogine, Quantum Zeno effect, *Phys. Lett. A* **151**, 109 (1990).
- [63] A. A. Clerk, M. H. Devoret, S. M. Girvin, F. Marquardt, and R. J. Schoelkopf, Introduction to quantum noise, measurement, and amplification, *Rev. Mod. Phys.* **82**, 1155 (2010).
- [64] M. H. Devoret and R. J. Schoelkopf, Amplifying quantum signals with the single-electron transistor, *Nature (London)* **406**, 1039 (2000).
- [65] A. N. Korotkov and D. V. Averin, Continuous weak measurement of quantum coherent oscillations, *Phys. Rev. B* **64**, 165310 (2001).
- [66] L. D. Landau and E. M. Lifshitz, *The Classical Theory of Fields* (Butterworth-Heinemann, Oxford, UK, 1975).
- [67] D. A. Varshalovich, A. N. Moskalev, and V. K. Khersonskii, *Quantum Theory of Angular Momentum* (World Scientific, Singapore, 1988).
- [68] K. De Greve, L. Yu, P. L. McMahon, J. S. Pelc, C. M. Natarajan, N. Y. Kim, E. Abe, S. Maier, C. Schneider, M. Kamp, S. Höfling, R. H. Hadfield, A. Forchel, M. M. Fejer, and Y. Yamamoto, Quantum-dot spin-photon entanglement via frequency downconversion to telecom wavelength, *Nature (London)* **491**, 421 (2012).
- [69] W. B. Gao, P. Fallahi, E. Togan, J. Miguel-Sanchez, and A. Imamoglu, Observation of entanglement between a quantum dot spin and a single photon, *Nature (London)* **491**, 426 (2012).
- [70] J. R. Schaibley, A. P. Burgers, G. A. McCracken, L.-M. Duan, P. R. Berman, D. G. Steel, A. S. Bracker, D. Gammon, and L. J. Sham, Demonstration of Quantum Entanglement between a Single Electron Spin Confined to an InAs Quantum Dot and a Photon, *Phys. Rev. Lett.* **110**, 167401 (2013).
- [71] W. K. Wootters, Entanglement of Formation of an Arbitrary State of Two Qubits, *Phys. Rev. Lett.* **80**, 2245 (1998).
- [72] F. Li, A. Saxena, D. Smith, and N. A. Sinitsyn, Higher-order spin noise statistics, *New J. Phys.* **15**, 113038 (2013).
- [73] D. S. Smirnov and K. V. Kavokin, Optical resonance shift spin-noise spectroscopy, *Phys. Rev. B* **101**, 235416 (2020).
- [74] K. Jacobs and D. A. Steck, A straightforward introduction to continuous quantum measurement, *Contemp. Phys.* **47**, 279 (2006).
- [75] D. Hägele and F. Schefczik, Higher-order moments, cumulants, and spectra of continuous quantum noise measurements, *Phys. Rev. B* **98**, 205143 (2018).
- [76] J. Wiegand, D. S. Smirnov, J. Hübner, M. M. Glazov, and M. Oestreich, Spin and reoccupation noise in a single quantum dot beyond the fluctuation-dissipation theorem, *Phys. Rev. B* **97**, 081403(R) (2018).
- [77] M. T. Rakher, N. G. Stoltz, L. A. Coldren, P. M. Petroff, and D. Bouwmeester, Externally Mode-Matched Cavity Quantum Electrodynamics with Charge-Tunable Quantum Dots, *Phys. Rev. Lett.* **102**, 097403 (2009).
- [78] P. Androvitsaneas, A. B. Young, C. Schneider, S. Maier, M. Kamp, S. Höfling, S. Knauer, E. Harbord, C. Y. Hu, J. G. Rarity, and R. Oulton, Charged quantum dot micropillar system for deterministic light-matter interactions, *Phys. Rev. B* **93**, 241409(R) (2016).
- [79] S. Sun, H. Kim, G. S. Solomon, and E. Waks, A quantum phase switch between a single solid-state spin and a photon, *Nat. Nanotechnol.* **11**, 539 (2016).
- [80] X. Ding, Y. He, Z.-C. Duan, N. Gregersen, M.-C. Chen, S. Unsleber, S. Maier, C. Schneider, M. Kamp, S. Höfling, C.-Y. Lu, and J.-W. Pan, On-Demand Single Photons with High Extraction Efficiency and Near-Unity Indistinguishability from a Resonantly Driven Quantum Dot in a Micropillar, *Phys. Rev. Lett.* **116**, 020401 (2016).
- [81] A. J. Bennett, J. P. Lee, D. J. P. Ellis, I. Farrer, D. A. Ritchie, and A. J. Shields, A semiconductor photon-sorter, *Nat. Nanotechnol.* **11**, 857 (2016).
- [82] P. M. Vora, A. S. Bracker, S. G. Carter, T. M. Sweeney, M. Kim, C. S. Kim, L. Yang, P. G. Brereton, S. E. Economou, and D. Gammon, Spin-cavity interactions between a quantum dot molecule and a photonic crystal cavity, *Nat. Commun.* **6**, 7665 (2015).
- [83] K. G. Lagoudakis, K. Fischer, T. Sarmiento, A. Majumdar, A. Rundquist, J. Lu, M. Bajcsy, and J. Vučković, Deterministically charged quantum dots in photonic crystal nanoresonators for efficient spin-photon interfaces, *New J. Phys.* **15**, 113056 (2013).
- [84] J. Miguel-Sánchez, A. Reinhard, E. Togan, T. Volz, A. Imamoglu, B. Besga, J. Reichel, and J. Estève, Cavity quantum electrodynamics with charge-controlled quantum dots coupled to a fiber Fabry–Perot cavity, *New J. Phys.* **15**, 045002 (2013).
- [85] S. Sun and E. Waks, Single-shot optical readout of a quantum bit using cavity quantum electrodynamics, *Phys. Rev. A* **94**, 012307 (2016).
- [86] S. Sun, H. Kim, G. S. Solomon, and E. Waks, Cavity-Enhanced Optical Readout of a Single Solid-State Spin, *Phys. Rev. Appl.* **9**, 054013 (2018).
- [87] J. Berezovsky, M. H. Mikkelsen, O. Gywat, N. G. Stoltz, L. A. Coldren, and D. D. Awschalom, Nondestructive optical measurements of a single electron spin in a quantum dot, *Science* **314**, 1916 (2006).
- [88] M. Atatüre, J. Dreiser, A. Badolato, and A. Imamoglu, Observation of Faraday rotation from a single confined spin, *Nat. Phys.* **3**, 106 (2007).
- [89] M. H. Mikkelsen, J. Berezovsky, N. G. Stoltz, L. A. Coldren, and D. D. Awschalom, Optically detected coherent spin dynamics of a single electron in a quantum dot, *Nat. Phys.* **3**, 770 (2007).
- [90] A. Nick Vamivakas, Y. Zhao, C.-Y. Lu, and M. Atatüre, Spin-resolved quantum-dot resonance fluorescence, *Nat. Phys.* **5**, 198 (2009).

- [91] A. N. Vamivakas, C.-Y. Lu, C. Matthiesen, Y. Zhao, S. Fält, A. Badolato, and M. Atatüre, Observation of spin-dependent quantum jumps via quantum dot resonance fluorescence, *Nature (London)* **467**, 297 (2010).
- [92] C.-Y. Lu, Y. Zhao, A. N. Vamivakas, C. Matthiesen, S. Fält, A. Badolato, and M. Atatüre, Direct measurement of spin dynamics in InAs/GaAs quantum dots using time-resolved resonance fluorescence, *Phys. Rev. B* **81**, 035332 (2010).
- [93] A. Delteil, W. B. Gao, P. Fallahi, J. Miguel-Sanchez, and A. Imamoglu, Observation of Quantum Jumps of a Single Quantum Dot Spin Using Submicrosecond Single-Shot Optical Readout, *Phys. Rev. Lett.* **112**, 116802 (2014).